Biomaterials Science

ROYAL SOCIETY OF CHEMISTRY

PAPER

View Article Online
View Journal

Cite this: DOI: 10.1039/d5bm01154j

Retinal hypoxia reversal with PLGA-oxygen nanobubbles

Anika Bushra, †[a,c] Wen Ren, †[b,c] Daniel Um,[b,c] Xiaoxue Han,[b,c] Michael Tsipursky[d,e,f] and Joseph Irudayaraj *[b,c,d,g,h]

Pathologies associated with retinal hypoxia, including diabetic retinopathy, central/branch retinal artery occlusion (CRAO/BRAO), central/branch retinal vein occlusion (CRVO/BRVO), retinopathy of prematurity, sickle cell retinopathy, *etc.*, have limited effective therapeutic intervention strategies. To address this shortcoming, herein we propose a biocompatible and biodegradable poly (lactic-*co*-glycolic acid) shell-based oxygen nanobubbles (PLGA-ONBs) platform, formulated with PLGA, polyvinyl alcohol (PVA), and $NaHCO_3$. The formulation of a novel PLGA-ONBs was proposed, and the synthesis process was optimized with respect to dependent (sonication power, PVA, and $NaHCO_3$ concentrations) and response (hydrodynamic diameter and oxygen capacity) variables. The optimized formulation has a concentration of $(13.8 \pm 0.01) \times 10^{10}$ particles per ml with a hydrodynamic diameter of 142.83 ± 11.46 nm, and oxygen loading capacity of 47.2 ± 2.4 mg L^{-1}. After 4 weeks of storage, the ONBs were found to have an oxygen concentration of 38.9 ± 2.9 mg L^{-1}, indicating excellent oxygen retention capability. The PLGA-ONBs tested *in vitro* in Muller and R28 retinal cell lines demonstrated excellent biocompatibility and potential to mitigate hypoxia. In addition, the PLGA-ONBs treatment on hypoxic cells demonstrated restoration of mRNA expression of three key hypoxic genes (HIF-1α, PAI-1, and VEGF-A) to normoxic states, indicating hypoxia reversal potential. Biosafety of the PLGA-ONBs was demonstrated in a rabbit model, demonstrating promise in clinical translation. The PLGA-ONBs developed exhibited excellent oxygen loading and retention, potential in hypoxia mitigation, and a safety profile that could be a promising route to treating ischemic diseases of the eye.

Received 31st July 2025,
Accepted 12th September 2025

DOI: 10.1039/d5bm01154j

rsc.li/biomaterials-science

Introduction

Retinal ischemia refers to the lack of blood circulation to the retina, leading to oxygen and nutrient deprivation, resulting in visual impairment, potentially leading to blindness.[1] Retinal hypoxia is a common outcome of ischemic retinal diseases, such as diabetic retinopathy,[2] central/branch retinal artery occlusion (CRAO/BRAO),[3] central/branch retinal vein occlusion (CRVO/BRVO),[3] retinopathy of prematurity,[4] sickle cell retinopathy,[5] *etc.* Unfortunately, these clinical conditions lack effective intervention strategies and result in vision impairment and blindness.[1] As a mitigative strategy for retinal ischemia-induced hypoxia, hyperbaric oxygen therapy (HBOT) is considered a viable option, where the patient is subjected to inhalation of 100% pure oxygen in a hyperbaric chamber pressurized at one atmosphere absolute pressure.[6,7] In this treatment strategy, the vitrous body is expected to be saturated with oxygen, which then can act as an oxygen reservoir for 1–2 days post-HBOT treatment.[8] While HBOT is recommended, it is not approved by regulatory bodies as a routine procedure to treat ischemic retinal diseases due to its obvious side effects, including fatigue, light-headedness, barotrauma, hearing loss, chronic osteomyelitis, and oxygen toxicity to the central nervous system, *etc.*[9–11] Furthermore, there is insufficient information on oxygen diffusion from the outer to the inner retinal layers. Due to these limitations, HBOT is not a standard of care to treat ischemic diseases of the eye.

[a]*Department of Chemical and Biomolecular Engineering, University of Illinois at Urbana-Champaign, Urbana, IL 61801, USA*
[b]*Department of Bioengineering, University of Illinois at Urbana-Champaign, Urbana, IL 61801, USA. E-mail: jirudaya@illinois.edu*
[c]*Biomedical Research Center in Mills Breast Cancer Institute, Carle Foundation Hospital, Champaign, IL 61801, USA*
[d]*Carle-Illinois College of Medicine, University of Illinois at Urbana-Champaign, Champaign, IL 61820, USA*
[e]*Vitreo-Retinal Surgery, Ophthalmology Department, Carle Foundation Hospital, Champaign, IL 61802, USA*
[f]*Revive Biotechnology, Inc., 60 Hazelwood Drive, EnterpriseWorks, Champaign, IL 61820, USA*
[g]*Beckman Institute, Carl Woese Institute of Genomic Biology, University of Illinois at Urbana-Champaign, Urbana, IL 61801, USA*
[h]*Cancer Center at Illinois (CCIL), University of Illinois at Urbana-Champaign, Urbana, IL 61801, USA*
† These authors contributed equally to this work.

An alternative to HBOT, that might have a similar effect, is the intravitreal injection of oxygen-saturated solutions, which can directly supply oxygen to the hypoxic retina. However, this strategy is not devoid of limitations, due to loss of oxygen during storage, and lack of controlled release capability with potential to generate reactive oxygen species (ROS) and elevation of intraocular pressure (IOP). A more effective approach could be the development of micro/nano delivery systems formulated with polymer, lipid, protein, or hybrid shells with oxygen entrapped within the core.[12–14] The use of oxygen nanobubbles (ONBs) instead of simply oxygen-saturated solutions can be a promising strategy due to their controlled release and excellent oxygen loading and retention capacity. One of the drawbacks associated with some of the existing works on ONBs is their transient nature. Although some studies have demonstrated strong evidence for weeks to months of stability of ONBs in solution,[15–17] it is not uncommon for these ONBs to disintegrate within minutes to hours after formulation.[18,19] Development of stable ONBs with extended shelf-life and controlled release properties will have excellent practical value and clinical significance in terms of treating ischemic diseases.

Various techniques have been explored to extend the lifetime of ONBs. The addition of perfluorocarbon (PFC) and its homologs is one of the most common methods to extend the oxygen release profile and enhance the oxygen loading capacity of ONBs.[20–22] However, the safety concerns associated with the use of PFCs, such as microvascular vasoconstriction, make this strategy not ideal for medical applications.[23–25] Another approach constitutes strengthening the shell to prolong the lifetime by utilizing lipid bilayer-based shells[26–28] and lipid-polymer hybrid shells.[29–31] ONBs made of lipid shells are more stable in terms of oxygen loading and retention capability, while functionalization of the lipids or incorporating polymers in the shell can enable targeted oxygen delivery.[32,33] Multilayered ONBs that are more stable with controlled release properties have been proposed.[34–36] For instance, in our previous works, we demonstrated dextran-based ONBs integrated with lipids as a potential strategy to mitigate retinal ischemia.[34,35] This effort substantiated the claim that hollow nanostructures are ideal for oxygen storage and sustained release and can be used as an adjuvant for ocular ischemia mitigation. Besides addressing ischemia of the eye, these ONBS were also utilized as an oxygen delivery source in wound healing hydrogels,[37,38] with an enhanced healing rate. Although ONBs with lipid cores are promising, several drawbacks exist. One of the main drawbacks of lipid-based ONBs is the lack of compactness of lipid shells, as they are reliant on the hydrophilic–hydrophobic interaction of the lipid molecules. Even with the incorporation of a polymer to increase the stability of the shell, its capacity to retain oxygen was not satisfactory. Additionally, the phase transition nature of lipids resulted in the fusion of multiple ONBs, resulting in aggregation. Therefore, lipid-based ONBs fortified with polymers are an improvement, but not ideal due to a lack of stability, shelf-life, and oxygen retention.

Poly (lactic-*co*-glycolic acid) (PLGA) is a biodegradable polymer known for its excellent biocompatibility. PLGA has been widely used to fabricate micro- and nano-structures for drug delivery.[39–41] It has also been used to construct hollow nanostructures suitable for drug loading, with a prolonged release profile.[42,43] Inspired by the functional use of PLGA nanostructures, in this work, we propose PLGA-ONBs, where the shell of the ONBs was formulated with PLGA polymers, and oxygen could be loaded in the inner core. One potential drawback of this approach with regard to polymeric nanoparticles is the necessity to dissolve them in organic solvents such as ethanol, ethyl acetate, or related reagents to facilitate solvation and synthesis.[33,34] We address this limitation with PLGA-ONBs by completely evaporating the ethyl acetate used for dissolving the PLGA after the hollow nanostructures were formed. The formulation was optimized based on the pH (by varying $NaHCO_3$ concentration), PVA concentration, and sonication power with respect to an optimal hydrodynamic diameter while maximizing the oxygen loading capacity. It should be noted that the oxygen retention capacity as well as the particle size of PLGA-ONBs could be influenced by synthesis conditions. By tuning these conditions, the size of ONBs was optimized to ~150 nm with optimal oxygen retention and loading capacity. The proposed PLGA-ONBs were assessed for their potential to mitigate hypoxia in two retinal cell lines, namely, Muller and R28. The PLGA-ONBs synthesized did not induce ROS and superoxide dismutase (SOD) when used *in vitro*. Additionally, gene expression studies indicated that PLGA-ONBs treatment (under hypoxia) was effective in downregulating key hypoxic genes (HIF-1α, PAI-1, VEGF-A) to normoxic levels. Ocular safety of PLGA-ONBs upon intravitreal administration in a rabbit eye model indicated that the PLGA-ONBs are safe, and no significant toxicity was observed even after four weeks of observation. We expect that PLGA-ONBs could pave the way for the development of improved polymeric ONBs that are safe and stable with excellent oxygen release properties for the treatment of retinal ischemia-induced hypoxia.

Experimental methods

Chemicals and reagents

Poly(D,L-lactide-*co*-glycolide), 50 : 50, IV 1.0 dl g^{-1} was obtained from Polysciences, Inc. (PA, US). Polyvinyl alcohol (PVA), dextrose, coumarin 6, and sodium chloride were purchased from Sigma-Aldrich (MO, US). Sodium bicarbonate and dibasic potassium phosphate were obtained from Mallinckrodt Chemicals (MO, US). Water for Injection (WFI) was purchased from B. Braun Medical Inc. (PA, US). Casein peptone was purchased from Remel Products (MA, US). Peptone S (soy peptone) was provided by BioWorld (OH, US). Ethyl acetate was obtained from Fisher Scientific (MA, US).

Synthesis of PLGA-ONBs

PLGA hollow structures were fabricated based on a previously reported protocol[44] with modifications. By varying $NaHCO_3$

concentration (pH variation), the shell of the PLGA-ONBs was tuned for optimal results.[42,43] Briefly, 50 mg of PLGA was dissolved in 1 mL of ethyl acetate, which was then vigorously stirred for 1 hour in an open container. Then 1 mL of PLGA ethyl acetate solution was added dropwise to 1 mL of aqueous solution of 5% (w/v) PVA and 2.5 mg mL^{-1} $NaHCO_3$ at 40 °C, followed by rapid addition of 1 mL of solution of 5% (w/v) PVA and 2.5 mg mL^{-1} $NaHCO_3$. Vigorous stirring was continued throughout the whole mixing process. The mixture was stirred at room temperature for 5 minutes, followed by sonication at 30 W for 2 minutes. The sonicated mixture was then added to 50 mL of 0.05% (w/v) PVA aqueous solution and stirred overnight. Then, every 10 mL of the prepared PLGA hollow nanostructures was transferred into a glass vial and dried, and purged with oxygen for 10 minutes at 5 psi to fill the vial with pure oxygen. The vial was sealed immediately and kept at 4 °C for 2 days for loading oxygen into the PLGA hollow structures through diffusion. Later, 6 mL of oxygen-saturated WFI was added to the vials with a syringe, and the vial was sonicated for 1 minute to redisperse the obtained PLGA-ONBs. The prepared PLGA-ONBs were loaded in 3 mL vials sealed with a rubber stopper and an aluminium cap with a manual crimper and stored at 4 °C until further use.

To synthesize fluorescent PLGA-ONBs, coumarin 6 was dissolved along with PLGA in ethyl acetate to obtain an ethyl acetate solution with 50 mg mL^{-1} of PLGA and 2 mg mL^{-1} of coumarin 6. The rest of the synthesis was the same as that with PLGA ethyl acetate solution under optimized conditions. The obtained fluorescent PLGA-ONBs were purified with dialysis (12 kDa MWCO). Due to the insolubility of coumarin 6 in water[45] and the purification, the coumarin 6 molecules are expected to be entrapped in the shells of the obtained fluorescent PLGA-ONBs. As shown in Fig. S1, the fluorescence from the dialysis solution after purification was extremely weak compared to that from fluorescent PLGA-ONBs, indicating an insignificant detachment of coumarin 6.

Total oxygen determination

To determine the total oxygen loaded in the PLGA-ONBs, a vacuum-based setup was utilized. First, 10 mL of water mixture was vacuumed at −20 inHg for 200 minutes. The oxygen concentration in the vacuumed water was determined with a Thermo Fisher Scientific Orion Versa Star Pro DO Benchtop Meter (Ontario, CA). Since the test range of the DO meter was 0–20 mg L^{-1} and the oxygen concentration in non-diluted PLGA-ONBs was greater than 40 mg L^{-1}, the test sample was diluted (25% dilution) before evaluation of oxygen concentration. Briefly, 2.5 mL of PLGA-ONBs was mixed with 7.5 mL of vacuumed (de-oxygenated) water, and the dilution was vacuumed at −20 inHg for 30 minutes to remove any oxygen that was present in the solution (not entrapped within PLGA-ONBs). The oxygen concentration of the vacuumed 25% (v/v) dilution of PLGA-ONBs was measured. Oxygenated WFI prepared by purging oxygen gas at 10 psi into WFI for 1 hour was used as a control. The oxygen concentration in the freshly prepared 25% dilution of oxygenated WFI was recorded. Then another batch of 25% (v/v) dilution of oxygenated WFI was vacuumed for 30 minutes at −20 inHg. The oxygen concentration in the vacuumed dilution of oxygenated WFI was measured. The total oxygen in the PLGA-ONBs was calculated based on the recorded oxygen concentrations above. A scheme of the total oxygen determination was illustrated in Fig. S2A. The experimental setup for the oxygen concentration is illustrated in Fig. S3.

Oxygen release test

The oxygen release profile of PLGA-ONBs was generated according to the method reported in our previous work with modifications.[34] Briefly, PLGA-ONBs samples were mixed at a ratio of 1 : 9 with deoxygenated WFI, prepared by purging nitrogen into WFI water at 10 psi for 1 hour. Then the mixture was immediately injected into an isolated glass tube where the optical probe of the DO meter was fixed as illustrated in Fig. S3. After the injection of the mixture, the glass tube was further sealed with parafilm. The oxygen concentration was monitored by the DO meter using a timed measurement model at 1 minute intervals. The measurement was performed at a room temperature of 21.04 ± 0.34 °C. Oxygenated WFI was tested following the same protocol as the control. The procedure for oxygen release is illustrated in Fig. S2B.

Characterizations of PLGA-ONBs

Dynamic light scattering (DLS) was used to determine the size and zeta potential of PLGA-ONBs at 10% (v/v) dilution in WFI with Anton Paar Litesizer 500 particle-sizing system (VA, US). The particle concentration was measured with Malvern Panalytical NanoSight NS300 (Nottingham, UK). Scanning electron microscopy (SEM) images were collected with FEI Quanta FEG 450 ESEM at 10.0 kV.

Sterility evaluation

The sterility of PLGA-ONBs was evaluated following the U.S. Pharmacopeia Sterility ⟨71⟩ specifications. Briefly, a soybean-casein digest medium was prepared with 1.7% (w/v) casein peptone, 0.5% (w/v) sodium chloride, 0.3% (w/v) Peptone S (soy peptone), 0.25% (w/v) dibasic potassium phosphate, and 0.23% (w/v) dextrose in 1 L of Biology grade water. The pH of the media was adjusted to 7.3 ± 0.2 with 1 M NaOH and then sterilized *via* autoclave. To investigate the sterility of PLGA-ONBs, 1 mL of prepared PLGA-ONBs was added to 9 mL of media in sterile 15 mL tubes. Biology grade water only and media only were used as two negative controls. For positive controls, media were inoculated with *Bacillus subtilis*, *Escherichia coli*, *Pseudomonas aeruginosa* 01, or *Pseudomonas aeruginosa* 14, respectively. The samples were incubated at room temperature, and the optical density (OD600) was measured daily with an Eppendorf Biophotometer. 1× PBS buffer was used as the blank. After 6 days, the positive controls appeared cloudy due to the consumption of nutrients and bacterial death, and the test was terminated after 14 days.

Cell culture

Muller cells (ENW001, Kerafast, Boston, MA) were cultured in DMEM (10–017-CV, Corning, Corning, NY) supplemented with 10% (v/v) fetal bovine serum (16140-071, Gibco, Waltham, MA), 1% (v/v) Pen-Strep (17-6020E, Lonza, Basel, Switzerland), and 1% (v/v) L-glutamine (3772, Carl Roth, Karlsruhe, Germany). For R28 retinal cells (EUR201, Kerafast), the culture medium included DMEM (10-013-CV, Corning), supplemented with 10% (v/v) bovine calf serum (30-2030, ATCC, Manassas, VA), 1× MEM nonessential amino acids (11140-050, Gibco), 1% (v/v) Pen-Strep, 15 mL of 7.5% (w/v) sodium bicarbonate (7412-12, Mallinckrodt Chemicals, St. Louis, MO), and 5 mL of 200 mM L-glutamine (3772, Carl Roth). All cells were incubated at 37 °C and 5% CO_2.

Evaluation of cytotoxicity

Muller and R28 cells were cultured overnight in 96-well plates at 10 000 cells per well. The following morning, PLGA-ONBs at concentrations of 5, 10, 25, or 50% (v/v) were added to the cells for a total of 24 hours. Then, the MTT (M6494, Invitrogen, Waltham, MA) assay was performed per the manufacturer's instructions. Each group had a total of eight replicates.

Hypoxia recovery

Muller and R28 cells were seeded in 96-well plates at a density of 10 000 cells per well and incubated overnight. The following day, cells were either maintained under normoxic conditions or exposed to 12 hours of hypoxia (5% O_2, 5% CO_2, 90% N_2) and treated with PLGA-ONBs at concentrations of 5, 10, 25, 50% (v/v), or no treatment. Cell viability was assessed using an MTT assay according to the manufacturer's protocol.

Cellular uptake studies

Fluorescently labeled ONBs were synthesized to evaluate cell uptake. Muller and R28 cells were cultured in a humidified incubator at 37 °C with 5% CO_2. Cells were seeded into 96-well plates at a density of 10 000 cells per well and allowed to adhere overnight. The next day, the medium was discarded, and cells were treated with fluorescent ONBs with 5, 10, 25, and 50% (v/v) concentrations. Cells were then incubated for an additional 6 hours, followed by washing three times with 1× PBS to eliminate non-internalized ONBs and lysis using 1% (v/v) Triton X-100 to release the internalized ONBs. Fluorescence intensities were recorded (E_x: 480 nm, E_m: 525 nm) using a microplate reader. Each experimental group included eight replicates.

For dark-field imaging, 10% (v/v) treatment group was chosen, and the same procedure was followed as previously mentioned in the cell uptake experiments. After incubating with fluorescent ONBs for 6 hours, cells were washed three times with 1× PBS and fixed with 4% paraformaldehyde. After fixation, the cells were washed again with 1× PBS and stained with DAPI (4′,6-diamidino-2-phenylindole; D1306, Invitrogen™, USA) for approximately 10 minutes. A final 1× PBS wash was performed to remove excess dye, and the samples were stored at 4 °C until imaging. Fluorescence images were captured using a Zeiss Axio Observer Z1 inverted microscope (Carl Zeiss AG, USA).

ROS and superoxide determination

The ROS and Superoxide Detection Assay Kit (ab139476, Abcam, Waltham, MA) was utilized to measure ROS and superoxide levels following the manufacturer's protocol. Muller and R28 cells were seeded in 96-well black-walled plates with clear bottoms and allowed to adhere overnight. The following day, cells were exposed to PLGA-ONBs at concentrations of 5, 10, 25, or 50% (v/v) for 24 hours under normoxic conditions. ROS enhancer pyocyanin was used as the positive control (350 μM), while the ROS inhibitor *N*-acetyl-L-cysteine (5 mM) was used as the negative control. Subsequently, the detection solution was added to the cells and incubated for 60 minutes at 37 °C. Fluorescence intensities were recorded for ROS (E_x: 488 nm, E_m: 520 nm) and superoxide (E_x: 550 nm, E_m: 610 nm) levels. Each treatment group was tested in quintuplicate.

Hypoxic gene expression

Cells were seeded at a density of 0.6×10^6 cells per well in a 6-well plate (n = 2) the day before the experiment. The next day, fresh media were added, and cells were treated with either 25% (v/v) PLGA-ONB or left untreated. The plates were placed in a humidified hypoxic chamber for 12 hours, following the same conditions as the experiments above. Then, cells were washed with 1× PBS, trypsinized, pelleted, and washed again with 1× PBS. Total RNA was extracted from each group using TRIzol reagent per the manufacturer's instructions. Complementary DNA (cDNA) was synthesized using the High-Capacity cDNA Reverse Transcription Kit (Applied Biosystems, 4368814, Waltham, MA). Quantitative real-time PCR (RT-qPCR) was conducted with the Power SYBR Green PCR Master Mix and the StepOnePlus Real-Time PCR System (Applied Biosystems), following the manufacturer's guidelines. The expression levels of hypoxia-inducible factor 1 alpha (HIF-1α), plasminogen activator inhibitor-1 (PAI-1), and vascular endothelial growth factor A (VEGF-A) were normalized to endogenous control glyceraldehyde-3-phosphate dehydrogenase (GAPDH). The primer sequences of each gene were as follows: GAPDH (forward [F]: 5′- TGA TTC TAC CCA CGG CAA GT-3′; reverse [R]: 5′- AGC ATC ACC CCA TTT GAT GT-3′), HIF-1α (F: 5′- GCA GAA TGC TCA GAG GAA GC-3′; R: 5′- ACG TTC CAA TTC CTG CTG CT-3′), PAI-1 (F: 5′-GGC ACA ATC CAA CAG AGA CAA TC-3′; R: 5′-AGG CTT CTC ATC CCA CTC TCA A-3′), and VEGF (F: 5′-ACT GGA CCC TGG CTT TAC TG-3′; R: 5′-ACG CAC TCC AGG GCT TCA TC-3′).

Animal intravitreal injection

All animal procedures were performed in accordance with the Guidelines for Care and Use of Laboratory Animals approved by the Animal Ethics Committee of the University of Illinois, Chicago. The ocular safety study was conducted under the protocol number 24-096-Modification 01 approved by the Office of

Animal Care and Institutional Biosafety (OACIB), under the protocol entitled "Acute and Repeat-dose Toxicity and Pharmacokinetics Studies in Rabbits". The study was conducted by the Toxicology Research Laboratory in the Department of Pharmacology, University of Illinois, Chicago, and strictly conformed to the Association for Research in Vision and Ophthalmology (ARVO) statement for the Use of Animals in Ophthalmic and Vision Research. Four male New Zealand White rabbits were injected with the first dose of 50 μl PLGA-ONBs intravitreally in the right eyes, and after 24 hours, the second dose of 50 μl PLGA-ONBs was administered. The left eyes were not injected and used as a no-treatment control group. IOP measurements and ophthalmic examinations were conducted from Day 0 (before injection) to Day 27. The ophthalmic examinations included conjunctival congestion, conjunctival swelling, conjunctival discharge, corneal vascular pannus, corneal opacity, corneal opacity area, inflammatory KP, aqueous cell, hypopyon, aqueous flare, fibrin strands, iris hyperemia, iris exfoliation, iris synechia, anterior lens capsule deposit, posterior lens capsule deposit, lens opacity, vitreous cell, vitreous haze, retinal vasculitis, and papillitis. The ophthalmic exam score was calculated as the sum of findings from the above-mentioned parameters. After 27 days, the rabbits were euthanized humanely, and the eyes were collected. The eye tissues were fixed with modified Davidson's fixative, followed by H&E staining.

Statistical analysis

Statistical analysis was performed with R Studio statistical software. The data were analyzed using a one-way ANOVA followed by a Tukey's *post-hoc* test for the determination of statistical significance. A *p*-value less than 0.05 was considered to be the standard for a significant difference.

Results and discussion

Scheme 1 illustrates the preparation procedure of PLGA-ONBs. The synthesis of PLGA hollow nanostructures was conducted based on a previously reported oil-in-water emulsion method.[44] Briefly, PLGA hollow nanostructures were synthesized, dried, and purged with pure oxygen gas. The purpose of drying is to evaporate the solvent, thus allowing oxygen gas loading through diffusion and entrapment within the PLGA hollow shells. This was followed by redispersion in oxygenated WFI, assisted with short-term sonication, resulting in the final product of PLGA-ONBs. In the PLGA-ONBs, oxygen exists in two forms: (i) dissolved oxygen in the solvent and (ii) oxygen loaded into the PLGA hollow nanostructures. Oxygen concentration measured with regular oxygen probes can only account for the oxygen dissolved in solution. The shell separates the oxygen retained in PLGA-ONBs from the oxygen probe; hence, a direct readout of oxygen was not a viable option. Furthermore, the release rate of oxygen from the PLGA-ONBs could be considerably slower and accompanied by a significant loss of oxygen during testing, resulting in an inaccurate estimation of the total oxygen content. An efficient method for accelerating oxygen release from ONBs is diluting them with deoxygenated water, leading to a low oxygen level in the surrounding, increasing the release rate.[34] However, this method can result in an extended release profile, which could extend for up to 12 hours under Standard Temperature and Pressure (STP). Meanwhile, the diffusion of oxygen through the shell is dependent on the difference in the partial pressure of oxygen in and outside the shell. Thus, the oxygen released from ONBs would increase the partial pressure of oxygen in the surrounding alongside a decrease in the partial pressure of oxygen in the ONBs. This suggests that the release of oxygen would gradually decrease and reach a steady state when equilibrium is established between the partial pressure of oxygen inside and outside of the ONBs. To address this issue with the previously reported oxygen quantification methodology, we introduce a vacuum-based protocol to accelerate the release of oxygen. When oxygenated WFI is vacuumed, the oxygen would dissipate in the air, resulting in a rapid decrease in oxygen concentration. In contrast, when PLGA-ONBs were vacuumed under the same conditions, the released oxygen from the ONBs is expected to make up for some of the loss. The difference in oxygen concentration between the oxygenated WFI and PLGA-ONBs could be attributed to the oxygen loaded in PLGA-ONBs. Based on the concept, the total oxygen was roughly estimated by the equation:

$$C_{\text{total}} = \left[\left(C_{\text{PLGA-ONBs after vacuum}} + C_{\text{oxygenated WFI}} - C_{\text{oxygenated WFI after vacuum}}\right) - 75\% \times C_{\text{vacuumed water}}\right] \div 25\%,$$

where C_{total} is the estimated total oxygen concentration in the non-diluted PLGA-ONBs, $C_{\text{PLGA-ONBs after vacuum}}$ is the oxygen concentration in the PLGA-ONBs after vacuum, $C_{\text{oxygenated WFI}}$ is the oxygen concentration in the oxygenated WFI before vacuum, and $C_{\text{oxygenated WFI after vacuum}}$ is the oxygen concentration in the oxygenated WFI after vacuum. $C_{\text{vacuumed water}}$ is the oxygen concentration in the water vacuumed for 200 minutes in advance. The term ($C_{\text{PLGA-ONBs after vacuum}}$ + $C_{\text{oxygenated WFI}}$ − $C_{\text{oxygenated WFI after vacuum}}$) accounts for total oxygen in 25% (v/v) dilution of PLGA-ONBs. After subtracting

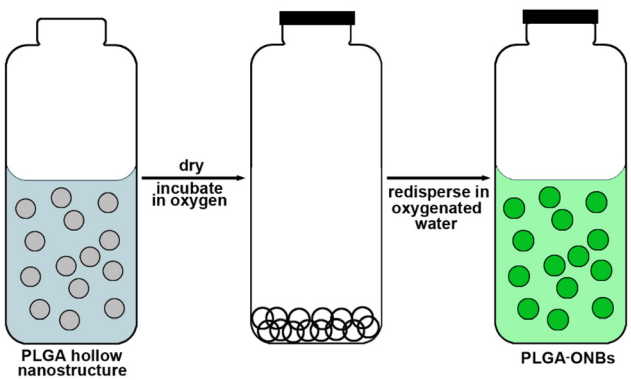

Scheme 1 Steps involved in the synthesis of PLGA-ONBs.

the amount of oxygen in the vacuumed water (which corresponded to 75% (v/v) of the solution), the total oxygen in the non-diluted PLGA-ONBs was determined. Compared with the previous oxygen diffusion quantification method based on the difference in partial pressure of oxygen, the vacuum-based method could enable faster oxygen release from the shells, thus providing a rapid route to evaluate the oxygen release profile of the obtained PLGA-ONBs.

The hydrodynamic diameter is a critical parameter for PLGA-ONBs bio-distribution, degradation in tissues, and is also expected to influence the total oxygen retention. One main contributing factor towards the size of ONBs is sonication power, since higher power signifies enhanced agitation, leading to a smaller particle size. The effect of sonication power variation (30, 40, and 70 W) on the size and oxygen retention is depicted in Fig. 1A and B, respectively. It can be seen that the size of the resulting PLGA-ONBs increases with higher sonication power (Fig. 1A). It might be because stronger sonication could induce the generation of smaller PLGA-ethyl acetate droplets, with a tendency to aggregate more than the larger droplets. The larger deviation in the size distribution shown in Fig. 1A is also an indicator of aggregation.

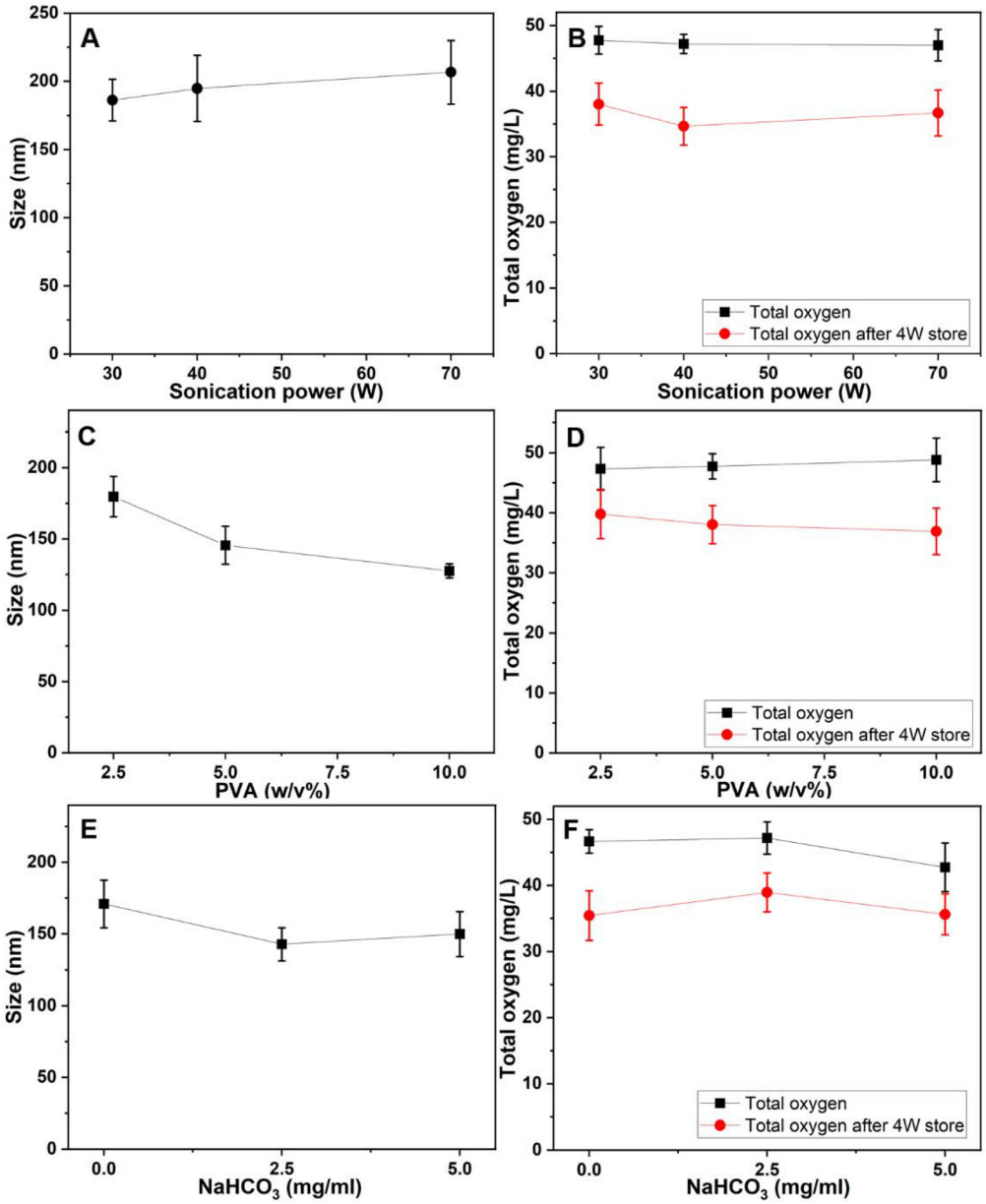

Fig. 1 PLGA-ONBs synthesis optimization. (A) The influence of the sonication power on the size, (B) the influence of sonication power on the total oxygen content, (C) the influence of PVA concentration on the size, (D) the influence of PVA concentration on total oxygen content, (E) the influence of $NaHCO_3$ concentration on the size, and (F) the influence of $NaHCO_3$ concentration on total oxygen content. Statistical analysis was performed using a one-way ANOVA followed by a Tukey's *post-hoc* test; data are presented as mean ± standard deviation (SD); $n = 3$.

Furthermore, the particle concentrations of the PLGA-ONBs synthesized at 30 W, 40 W, and 70 W were $11.1 \pm 0.05 \times 10^{10}$ particles per ml, $15.1 \pm 0.07 \times 10^{10}$ particles per ml, and $13.9 \pm 0.05 \times 10^{10}$ particles per ml, respectively. Since there is no significant difference in particle concentration with respect to a change in sonication power, this substantiates the claim that with higher sonication power, the particles are aggregated, resulting in an increase in the hydrodynamic diameter. However, the aggregation of PLGA-ethyl acetate droplets is expected to influence the generation of hollow nanostructures. In Fig. 1B, it is noted that the total oxygen in PLGA-ONBs freshly synthesized under different sonication powers is higher than 45 mg L^{-1}. In contrast, the total oxygen in oxygenated water was only 32.0 ± 1.2 mg L^{-1}. The comparison between the total oxygen in PLGA-ONBs and oxygenated water clearly illustrates the oxygen loaded in PLGA-ONBs. Furthermore, it can be seen that with higher sonication power, the oxygen retention capacity of the PLGA-ONBs after 4 weeks storage decreases. Based on these observations, 30 W sonication power was chosen as the optimal one.

To estimate the influence of the PVA concentration, the synthesis was conducted with 2.5, 5, and 10% (w/v) PVA. The change in size with respect to PVA concentration is shown in Fig. 1C. It can be seen that with an increase in PVA concentration, the size of the obtained PLGA-ONBs decreased from 179.63 ± 14.14 nm to 127.45 ± 4.98 nm. Meanwhile, the particle concentration of the obtained PLGA-ONBs changed from $(11.2 \pm 0.03) \times 10^{10}$ (PVA at 2.5%), $(17.4 \pm 0.01) \times 10^{10}$ (PVA at 5%) to $(17.8 \pm 0.07) \times 10^{10}$ (PVA at 10%). Interestingly, the total oxygen content did not vary significantly with a change in PVA concentration (Fig. 1D). We suggest that with an increase in PVA concentration, particle size is reduced (Fig. 1C), but concentration is increased, with the overall PLGA-shell inner volume remaining significantly similar, leading to comparable oxygen levels. After a 4 week storage, it is noted that the oxygen concentration in all the groups decreased, while oxygen loss in the larger PLGA-ONBs, *e.g.*, the batch synthesized with 2.5% (w/v), was smaller compared with other groups (Fig. 1D), indicating that larger PLGA-ONBs may be able to withhold more oxygen, compensating for the loss of oxygen during storage. On the other hand, considering the fact that smaller nanoparticles are expected to diffuse faster when injected into tissues, this might result in expedited oxygen delivery. Meanwhile, a shorter half-life is expected for smaller PLGA nanoparticles. Thus, the PLGA-ONBs synthesized with 5% (w/v) PVA were chosen as optimal, balancing the oxygen withholding capacity and circulation half-life.

Another important parameter that might influence the formation of hollow structures is $NaHCO_3$, which could generate gas in an acidic environment, thus assisting in the formation of hollow structures. Considering the pK_a value of PVA[46] is 4.7, it was expected that the addition of $NaHCO_3$ may aid in the formation of hollow structures, thus leading to improved oxygen loading and release. To test this hypothesis, we carried out the synthesis with 2.5 mg mL^{-1} and 5 mg mL^{-1} $NaHCO_3$. The size and the oxygen retention capacity are plotted in Fig. 1E and F, respectively. A decrease in the shell size with 2.5 mg mL^{-1} of $NaHCO_3$ is noted in Fig. 1E compared with PLGA-ONBs without $NaHCO_3$, suggesting that the addition of $NaHCO_3$ may influence the size of the PLGA-ethyl acetate droplets, along with the formation of shells. When the concentration of $NaHCO_3$ was increased to 5 mg mL^{-1}, no further change in size was noted compared to the 2.5 mg mL^{-1} batch. Fig. 1F showed that the addition of 2.5 mg mL^{-1} of $NaHCO_3$ increased the oxygen retention capacity of the freshly prepared and stored PLGA-ONBs compared to those without $NaHCO_3$, indicating ease of oxygen loading. However, when the added $NaHCO_3$ was increased to 5 mg mL^{-1}, the capacity of oxygen retention of the obtained PLGA-ONBs decreased, implying that a higher level of $NaHCO_3$ might partly weaken the shell and compromise oxygen retention.

Based on experiments, PLGA-ONBs synthesized under 30 W with 5% PVA and 2.5 mg mL^{-1} $NaHCO_3$ were considered optimal and used for the subsequent *in vitro* and *in vivo* investigations. The hydrodynamic diameter was 142.83 ± 11.46 nm, the concentration of ONBs was $13.8 \pm 0.01 \times 10^{10}$ particles per ml, with a zeta potential of -14.5 ± 0.6 mV. As shown in Fig. 1B, D and F, the total oxygen in PLGA-ONBs samples remained similar over a 4 week storage period, indicating that the proposed PLGA-ONBs could retain entrapped oxygen in the samples for at least 4 weeks when kept in sealed vials at 4 °C. Under the mentioned storage conditions, the diffusion of oxygen from PLGA-ONBs is expected to be minimized, leading to minimal oxygen loss. An image of the optimized PLGA-ONBs in a sealed glass vial is shown in Fig. 2A. It can be seen that the obtained PLGA-ONBs sample is a cloudy, pale white solution. The SEM images in Fig. 2B and C illustrate that the PLGA ONBs are spherical at around 140–170 nm, and the size distribution is uniform. To further characterize the size distribution of the PLGA-ONBs, DLS was utilized, and the corresponding size distribution curve is shown in Fig. 2D. A strong peak in the range between 0–10 000 nm (Fig. 2D and the inset figure in Fig. 2D), indicates good uniformity in the size of PLGA-ONBs without aggregation. Based on the DLS results, the optimized PLGA-ONBs have a hydrodynamic diameter of 142.83 ± 11.46 nm with a polydispersity index (PDI) of $15.75 \pm 2.37\%$.

Fresh PLGA-ONBs with an oxygen loading capacity of about 47.2 mg L^{-1} were stored at 4 °C to prevent oxygen loss to the surroundings. At 4 °C, the oxygen saturation is 74.3%, which is less than 100%; thus, the oxygen will transfer from the surrounding to the PLGA-ONBs samples to increase the oxygen level. At the ambient temperature of 25 °C, 47.2 mg L^{-1} oxygen corresponds to 119.6% oxygen saturation. Thus, PLGA-ONBs stored at ambient temperature will lose oxygen over time. In oxygen-saturated environments, as the oxygen inside and outside the PLGA shells are in equilibrium, there will be no loss of oxygen from the ONBs. At a physiological temperature of 37 °C, 47.2 mg L^{-1} oxygen corresponds to 147.8% oxygen saturation. This signifies that there will be oxygen loss from the PLGA-ONBs under physiological conditions, and the release rate of oxygen will be much higher than at ambient

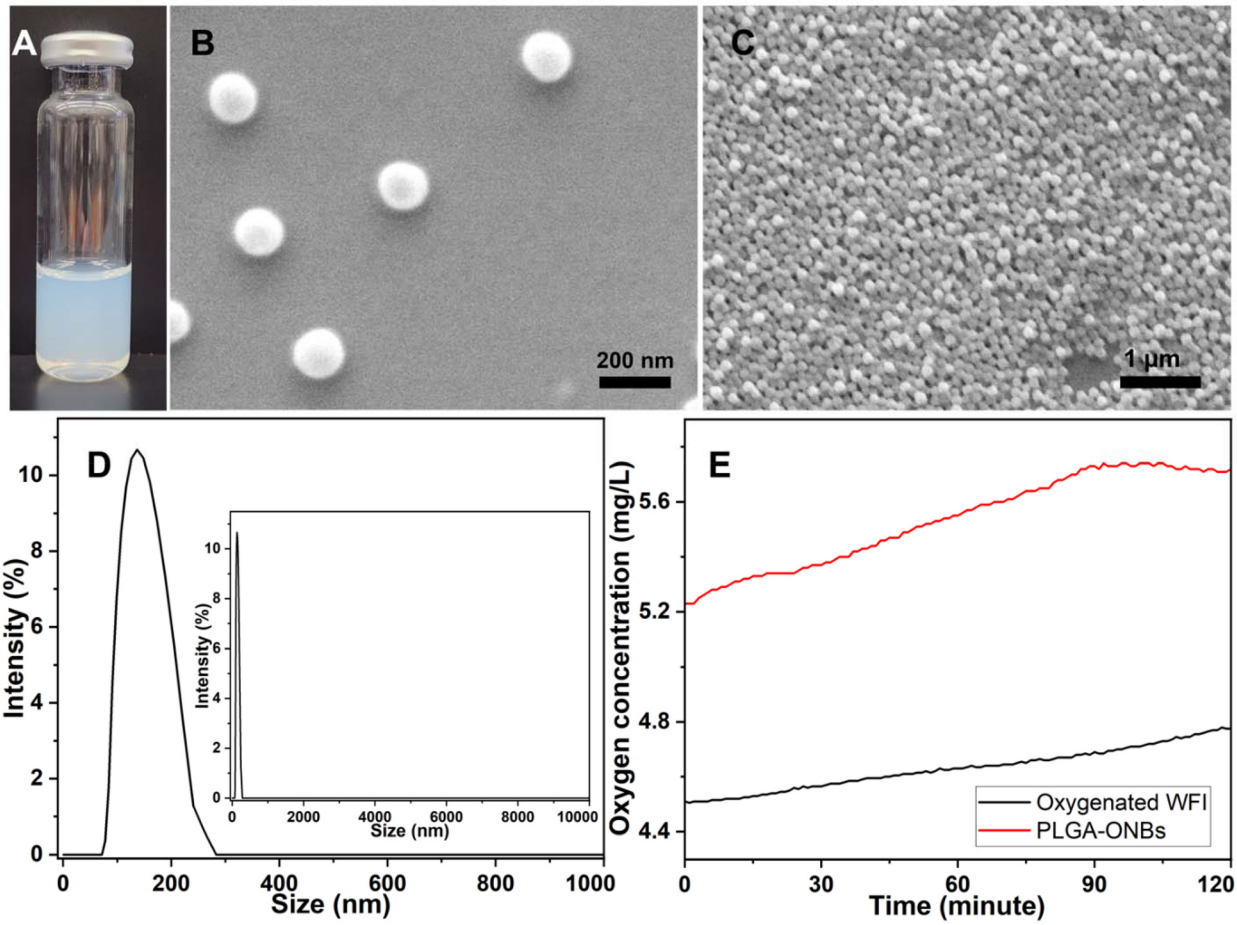

Fig. 2 PLGA-ONBs characterization. (A) Image of freshly prepared PLGA-ONBs in sealed glass vial, (B) SEM image (scale bar = 200 nm), (C) SEM image (scale bar = 1 μm), (D) size distribution of the optimized PLGA-ONBs synthesized under 30 W with 5% PVA and 2.5 mg mL^{-1} $NaHCO_3$, and (E) oxygen release profile of PLGA-ONBs in deoxygenated water at a ratio of 1 : 9 along with oxygenated WFI as the control.

temperature. Thus, when injected into the eyes, the physiological temperature is expected to induce a faster oxygen release to rescue the cells from hypoxia.

To investigate the oxygen release behavior of the optimized PLGA-ONBs, the oxygen concentration in the mixtures of PLGA-ONBs and deoxygenated water at a ratio of 1 : 9 was recorded. The deoxygenated water was chosen to simulate an ischemic environment to demonstrate the oxygen-releasing ability of PLGA-ONBs in hypoxic conditions. The resulting mixture at low oxygen levels is expected to facilitate the oxygen release from PLGA-ONBs, enabling a clear demonstration of the oxygen release behavior. The oxygen concentration in deoxygenated water prepared by purging nitrogen into DI water for 1 hour was evaluated to be 2.45 ± 0.24 mg L^{-1}. The initial oxygen concentration in the mixtures of PLGA-ONBs and deoxygenated water is 5.48 ± 0.32 mg L^{-1}, indicating a rapid increase in the oxygen level due to the addition of PLGA-ONBs, which could be attributed to the dissolved oxygen in the PLGA-ONBs samples. It can be observed in Fig. 2E that the oxygen concentration slowly increased for ~90 minutes and then became stable, depicting a saturation state. Oxygenated WFI was tested using the same protocol as the control. A slight increase in oxygen concentration in the profile from the control can be attributed to the leak of oxygen from the environment to the test system. Based on the volume of the test system (~4.5 mL), the amount of oxygen that entered the system due to the leak is calculated to be around 0.81 μg. The oxygen release from PLGA-ONBs during the 90 minute release is thereby calculated to be ~1.49 μg, (2.30–0.81) μg. Combined with the contribution of the dissolved oxygen in PLGA-ONBs, the total oxygen from the samples is estimated to be around 13.64 μg from dissolved oxygen, (5.48–2.45) mg L^{-1} × 4.5 ml, and oxygen release from PLGA-ONB particles, 1.49 μg. This 13.64 μg of oxygen is a more conservative estimate of the total oxygen determined by the vacuum-based method, which should be attributed to the fact that the oxygen release would be more under −20 inHg than that under ambient pressure.

The sterility of the optimized PLGA-ONBs was investigated following the Pharmacopeia Sterility Tests ⟨71⟩. The optical density (OD600) was plotted over the experiment duration of 14 days in Fig. 3. The positive control groups, media with *Bacillus subtilis*, *Escherichia coli.*, *Pseudomonas aeruginosa* 01,

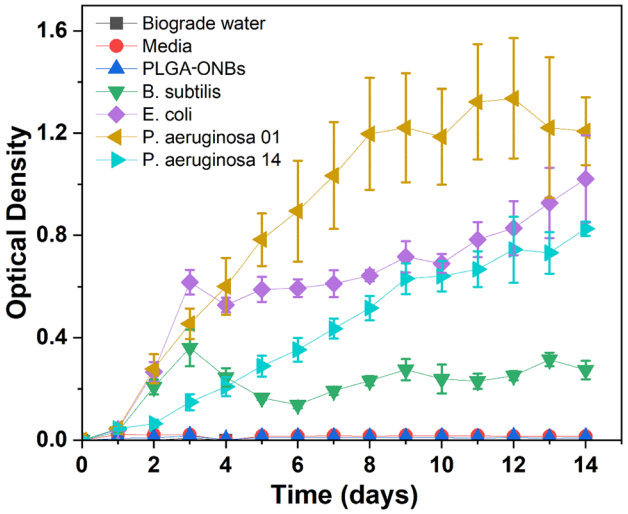

Fig. 3 Evaluation of sterility for the optimized PLGA-ONBs. Data are presented as mean ± standard deviation (SD); $n = 5$.

or *Pseudomonas aeruginosa* 14, exhibited clear bacterial growth. In contrast, the PLGA-ONBs group showed no bacterial growth consistently throughout the study period, demonstrating the sterility of PLGA-ONBs.

In vitro safety and efficacy of the proposed PLGA-ONBs were evaluated in two retinal cells, Muller, a principal glial retinal cell line, and R28, a retinal precursor cell line. To ensure the biocompatibility of the PLGA-ONBs, cytotoxicity experiments were performed with Muller (Fig. 4A) and R28 (Fig. 4B) cells under normoxic conditions, and viability was quantified with the MTT assay. Fig. 4 demonstrates the viability of cells treated with PLGA-ONBs at concentrations of 5, 10, 25, or 50% (v/v) after 24 hours of treatment. Though minimal cytotoxicity was observed in cells treated with higher concentrations of PLGA-ONBs, such as 25 or 50% (v/v), overall, there was no significant difference between the viability of the no-treatment group *versus* the treatment groups. Muller cells exhibited consistent cell viability after PLGA-ONB treatment, with results comparable to untreated controls across all concentrations. This indicates that PLGA-ONBs could be well tolerated by Muller cells, even at higher doses. In R28 cells, PLGA-ONBs showed greater biocompatibility at lower concentrations. However, a slight decline in viability was observed at the highest concentration; however, this decrease was not statistically significant compared to the no-treatment group. Overall, these findings demonstrate that PLGA-ONBs are non-cytotoxic and biocompatible, making them a promising candidate in therapeutic applications in retinal hypoxia reversal.

To evaluate the ability of PLGA-ONBs in hypoxia reversal, cells maintained under hypoxic conditions for 12 hours were treated with 5, 10, 25, and 50% (v/v) of PLGA-ONBs. As shown in Fig. 5, hypoxia treatment significantly reduced cell viability across both cell lines compared to normoxic controls ($p < 0.05$). PLGA-ONBs demonstrated dose-dependent hypoxia reversal efficacy, with 5% and 10% (v/v) of PLGA-ONBs significantly improving viability compared to the no-treatment group under hypoxic conditions. The 10% (v/v) PLGA-ONBs treatment group consistently showed the highest efficacy in restoring viability under hypoxic conditions back to levels comparable to the normoxic no treatment group. However, it should also be noted that at high concentrations of PLGA-ONBs, diminished viability was observed in both Muller (Fig. 5A) and R28 (Fig. 5B) cells, which could be attributed to excessive oxygen levels (hyperoxia) or potential aggregation effects, which may interfere with cellular functions. These results demonstrate consistent hypoxia reversal efficacy of 10% (v/v) PLGA-ONBs treatment, suggesting a balance between effective cellular oxygen delivery with minimal cytotoxicity.

To investigate cellular uptake, fluorescent ONBs were incubated with Muller and R28 cells for six hours. ONB uptake was quantified using a microplate reader to demonstrate dose-dependent PLGA-ONB uptake (Fig. 6A). Additionally, fluorescent images were captured to visualize the ONBs taken by

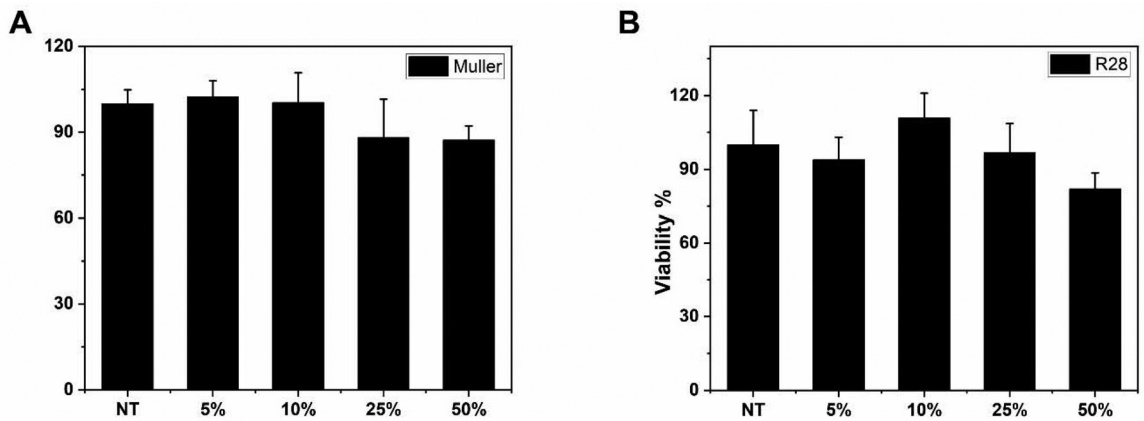

Fig. 4 Cytotoxicity evaluation of PLGA-ONBs. (A) MTT assay results for Muller cells, and (B) MTT assay results for R28 cells treated with serial concentrations of PLGA-ONBs. Statistical analysis was performed using a one-way ANOVA followed by a Tukey's *post-hoc* test; data are presented as mean ± standard deviation (SD); $n = 6$. "n.s." indicates no significant difference between groups.

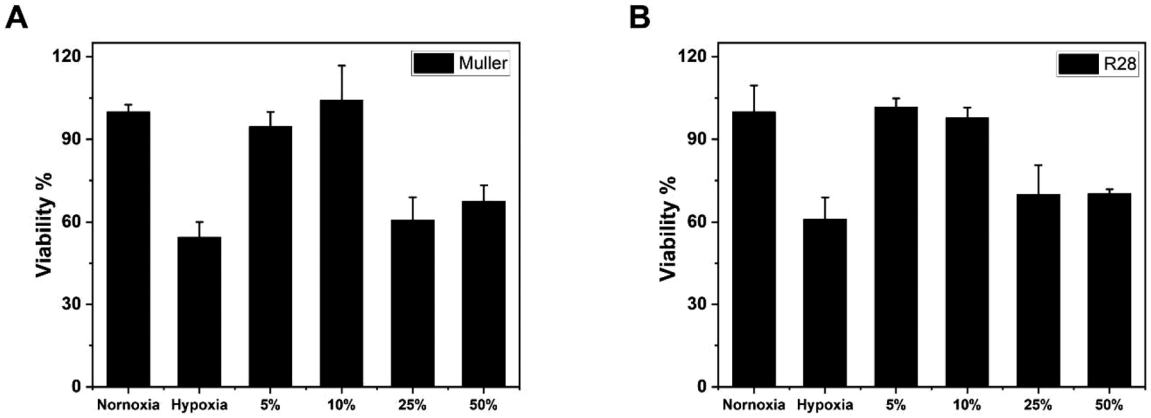

Fig. 5 Hypoxia recovery with PLGA-ONBs treatment. (A) Hypoxia recovery in Muller cells, and (B) hypoxia recovery in R28 cells cultured under hypoxia (5% O_2) for 12 hours. Statistical analysis was performed using a one-way ANOVA followed by a Tukey's *post-hoc* test; data are presented as mean ± standard deviation (SD); $n = 4$. "n.s." indicates no significant difference between groups. *$p < 0.05$, and **$p < 0.01$.

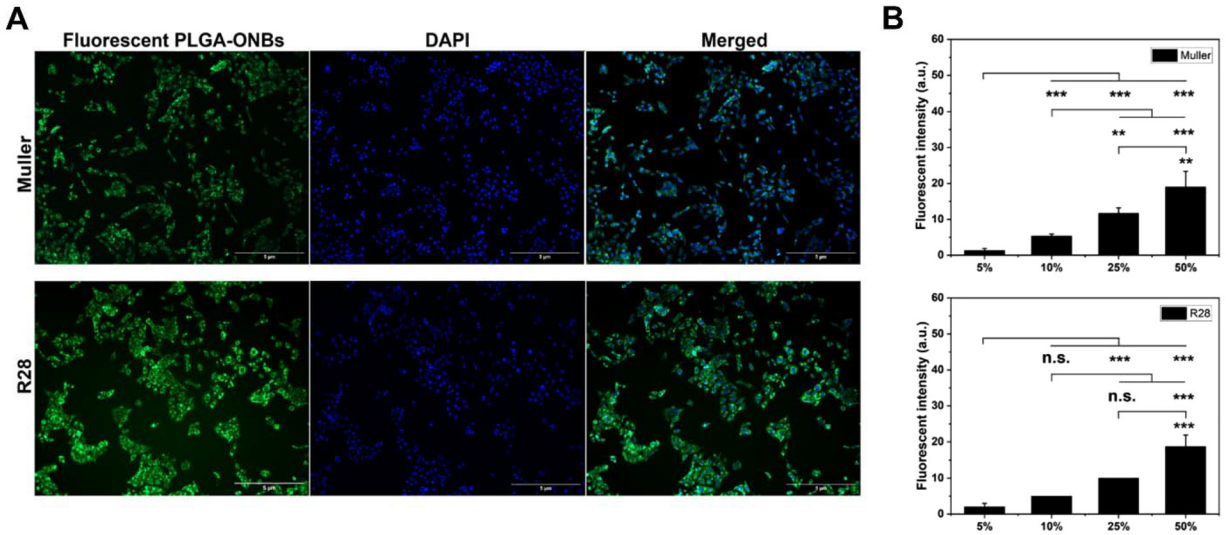

Fig. 6 Uptake of coumarin-6 labelled PLGA-ONBs. (A) Quantification of cell uptake in Muller and R28 cells, and (B) Darkfield images for Muller and R28 cells with uptaken fluorescent ONBs. Statistical analysis was performed using a one-way ANOVA followed by a Tukey's *post-hoc* test; data are presented as mean ± standard deviation (SD); $n = 4$. "n.s." indicates no significant difference between groups. **$p < 0.01$, and ***$p < 0.001$.

the cells (Fig. 6B). For both Muller and R28 cells, an increase in the uptake of ONBs was observed at higher treatment concentrations, indicating dose-dependency. Moreover, dark-field images for the 10% (v/v) treatment group confirmed successful uptake across most of the cell population and uniform distribution of the ONBs. Compared with the oxygen released in extracellular fluid, which could diffuse into cells only when the oxygen level in extracellular fluid is higher than inside the cells, the PLGA-ONBs have demonstrated direct intracellular oxygen delivery potential, negating dependency on oxygen level in the cells. Therefore, it is believed that besides extracellular release and subsequent diffusion of oxygen into cells, the endocytosis of PLGA-ONBs also has a significant contribution to hypoxia reversal.

A potential concern in using PLGA-ONBs is the generation of ROS and SOD, due to excessive oxygenation. We tested the ROS and SOD levels in the cells treated with 5, 10, 25, and 50% (v/v) of PLGA-ONBs with pyocyanin as the positive control and *N*-acetyl-L-cysteine (NAC) as the negative control (Fig. 7). It can be seen that the ROS and SOD in the cells treated with PLGA-ONBs are significantly less than those of the positive control, indicating that the PLGA-ONBs are not likely to generate a significantly higher level of ROS or SOD. Additionally, most of the groups treated with PLGA-ONBs exhibited statistically similar levels of ROS and SOD compared with the negative control group, ROS inhibitor *N*-acetyl-L-cysteine, suggesting a low ROS and SOD generation when treated with PLGA-ONBs.

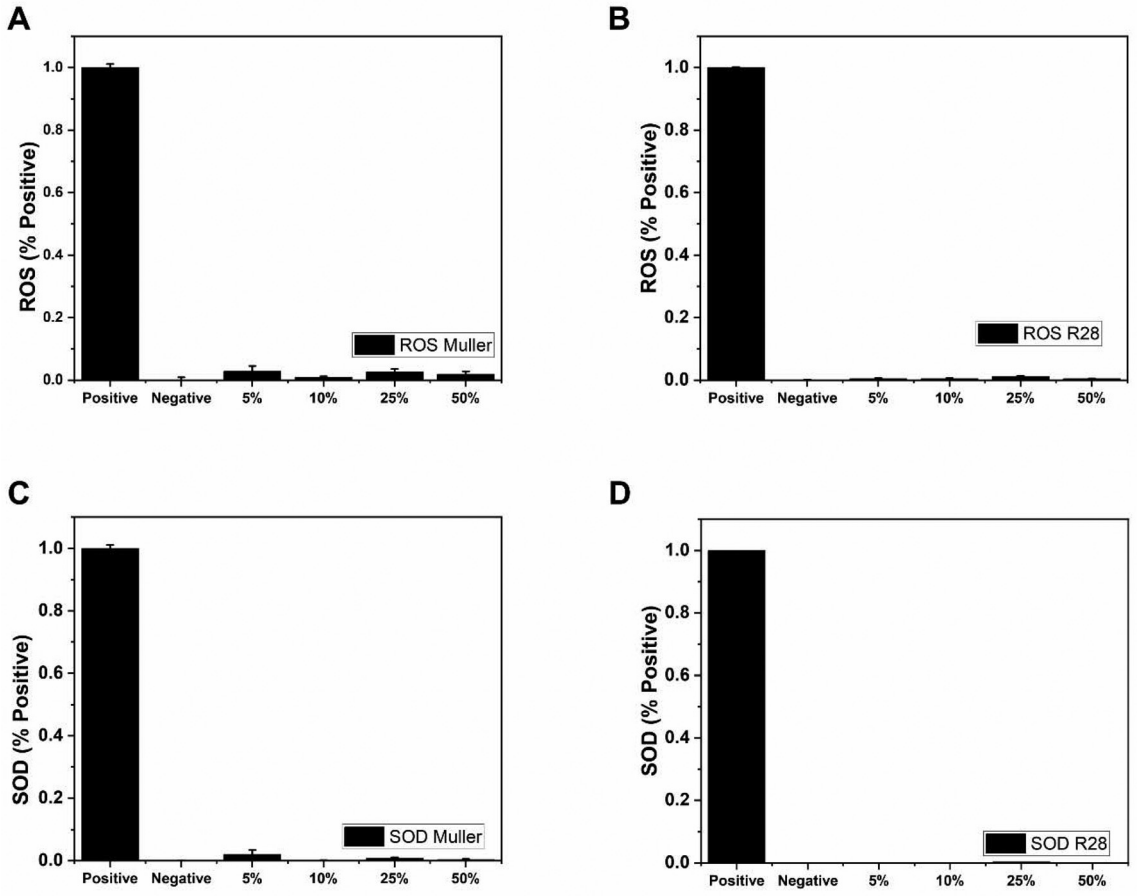

Fig. 7 ROS and SOD quantification for Muller and R28 cells treated with serial concentrations of PLGA-ONBs. (A) ROS quantification in Muller cells, (B) ROS quantification in R28 cells, (C) SOD quantification in Muller cells, and (D) SOD quantification in R28 cells. Statistical analysis was performed using a one-way ANOVA followed by a Tukey's *post-hoc* test; data are presented as mean ± standard deviation (SD); $n = 5$. "n.s." indicates no significant difference between groups. *$p < 0.05$, and **$p < 0.01$.

To evaluate the influence of oxygen released from PLGA-ONBs on select hypoxic genes, namely, HIF-1α, PAI-1, and VEGF-A, mRNA expression was assessed. HIF-1α regulates the activation of downstream genes that produce proteins involved in angiogenesis and the anaerobic metabolism of cells in a low-oxygen environment, and is upregulated under

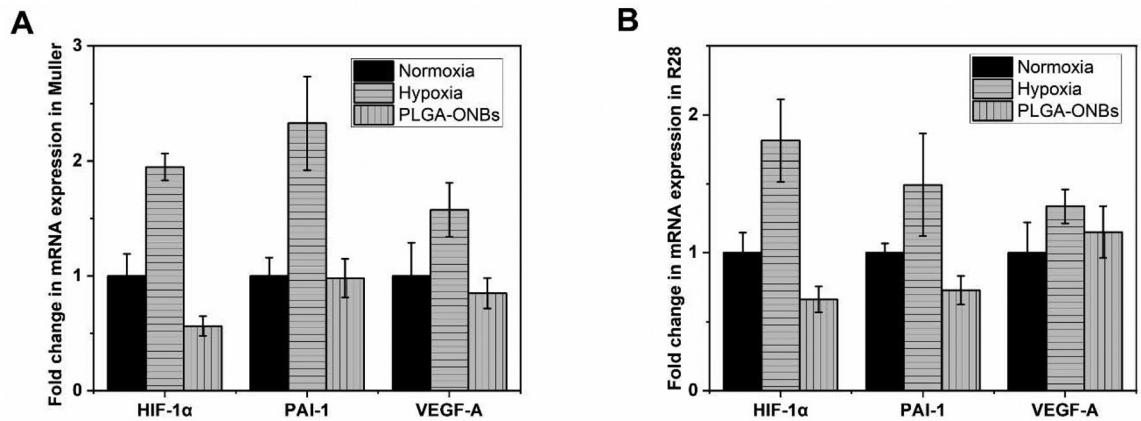

Fig. 8 Modulation of hypoxic genes with PLGA-ONBs treatment. Relative mRNA expression in cells under normoxic and hypoxic conditions and in PLGA-ONBs-treated cells under hypoxic conditions for (A) Muller cells, and (B) R28 cells. Statistical analysis was performed using a one-way ANOVA followed by a Tukey's *post-hoc* test; data are presented as mean ± standard deviation (SD); $n = 3$. "n.s." indicates no significant difference between groups. *$p < 0.05$, and **$p < 0.01$.

hypoxic conditions.[47,48] Another gene upregulated under hypoxic conditions is PAI-1, which inhibits the breakdown of fibrin.[49,50] VEGF-A is a direct downstream gene of HIF-1α, involved in angiogenesis, and is upregulated when cells are in hypoxic conditions.[51,52] For both Muller (Fig. 8A) and R28 (Fig. 8B) cells, expression of HIF-1α, PAI-1, and VEGF-A was upregulated in the cells incubated under hypoxic conditions compared to those under normoxic conditions. It is evident from Fig. 8 that PLGA-ONBs treatment resulted in a reduction in the expression of HIF-1α, PAI-1, and VEGF-A in both Muller (Fig. 8A) and R28 (Fig. 8B), indicating hypoxia mitigation. The inhibition in gene expression upon treatment with PLGA-ONBs demonstrates the potential of the developed ONBs to rescue the cells from hypoxia.

To evaluate *in vivo* safety, PLGA-ONBs were intravitreally injected into rabbit eyes. With no treatment group as the nega-

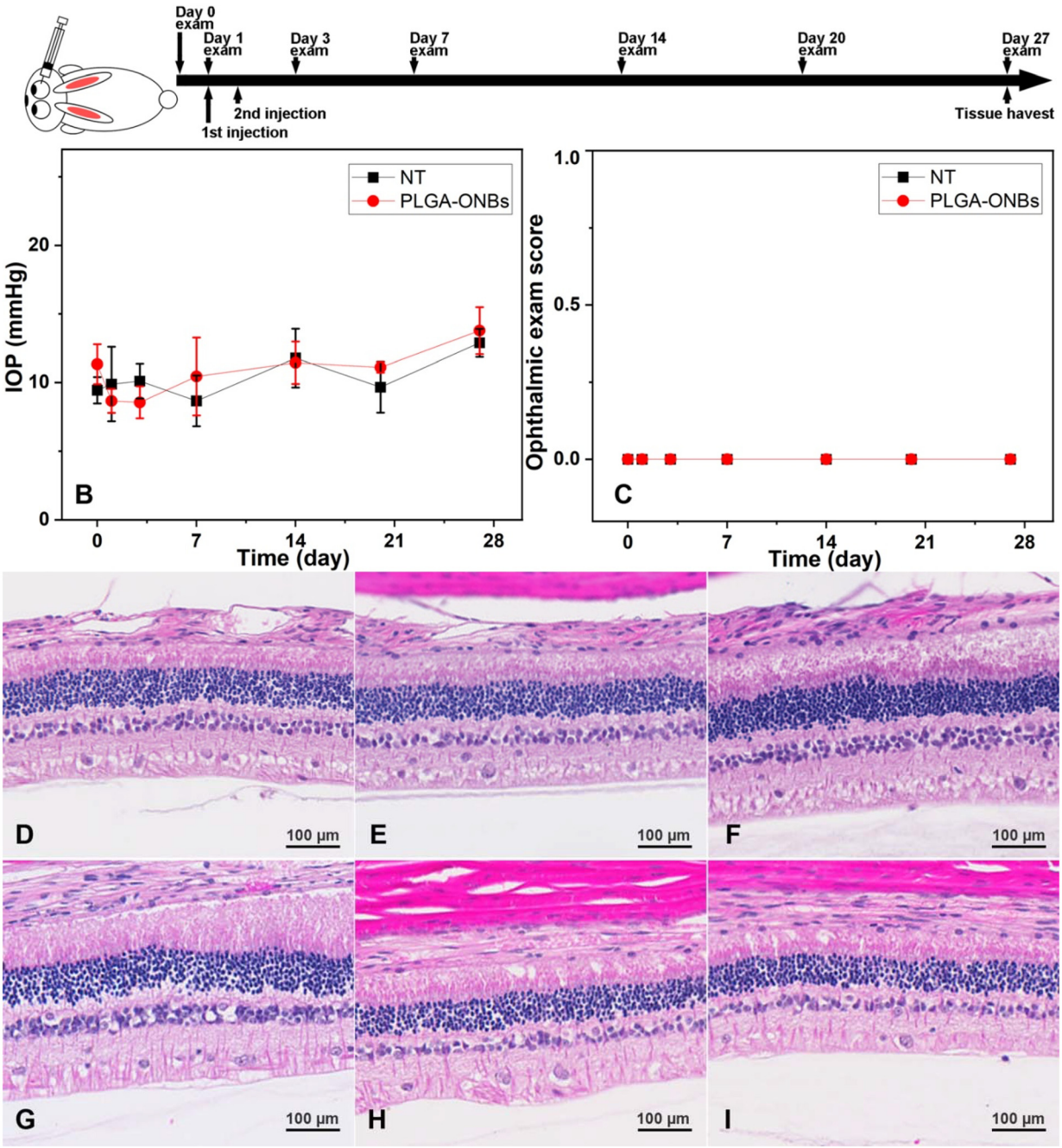

Fig. 9 *In vivo* ocular safety evaluation. (A) Scheme of intravitreal injection and examination timeline, (B) variation of IOP over the study period, (C), ophthalmic exam scores over the study period, (D–F) representative H&E stained histology images from eyes treated with PLGA-ONBs, and (G–I) representative H&E stained histology images from non-treated eyes as control. Statistical analysis was performed using a one-way ANOVA followed by a Tukey's *post-hoc* test; data are presented as mean ± standard deviation (SD); $n = 4$.

tive control, IOP (the fluidic pressure) and ophthalmic exam score were chosen as indicators of ocular safety. From Fig. 9A, the IOP level of the eyes injected with PLGA-ONBs was similar to that of the control group. Ophthalmic exam score was calculated as the sum of a series of ophthalmic examinations designed to indicate overall eye condition. In Fig. 9B, the PLGA-ONBs injected eyes showed a score of zero in most examination time points, implying no observable side effects due to PLGA-ONBs administration. The increase in the score on Day 1 in one subject was due to the slight conjunctival discharge in that animal. However, complete recovery was achieved before the examination on Day 3. Ocular safety profile of PLGA-ONBs was ascertained based on similar IOPs to control groups and low ophthalmic exam scores throughout the study. The histological evaluation of the eye tissues for the PLGA-ONBs-treated group and the control group further substantiated the ocular safety of the PLGA-ONBs. It can be seen that there is no observable difference in the retinal ganglion cell layer, inner nuclear layer, and outer nuclear layer between the PLGA-ONBs-treated group and the no-treatment group, further demonstrating the safety of the PLGA-ONBs, substantiating the potential candidacy of PLGA-ONBs as a viable alternative to treat ischemic diseases of the eye. Further *in vivo* evaluation of PLGA-ONBs in retinal ischemic disease-specific models is the next step to establish the proposed oxygen delivery platform as a therapeutic tool for a specific retinal ischemic condition.

Conclusion

In vitro efficacy of PLGA-ONBs was evaluated for retinal hypoxia reversal, and *in vivo* ocular safety was demonstrated in a rabbit model. The formulation protocol for the PLGA-ONBs synthesis was optimized for maximizing oxygen retention capacity and minimizing the hydrodynamic diameter. It was noted that a high sonication power during the synthesis would result in decreased oxygen retention, while an increase in the PVA concentration can lead to a reduction in the size of PLGA-ONBs. The addition of $NaHCO_3$ was found to aid the oxygen loading and retention capacity of the PLGA-ONBs. The amount of oxygen was estimated to be 47.2 ± 2.4 mg L^{-1}, which is much higher than that in fresh oxygenated water, 32.0 ± 1.2 mg L^{-1}. The amount of oxygen in PLGA-ONBs after a 4 week storage period was found to be 38.9 ± 2.9 mg L^{-1}, which was still higher than the oxygen level in fresh oxygenated water, indicating excellent oxygen retention capacity of the proposed PLGA-ONBs. Experiments with the synthesized ONBs in Muller and R28 retinal cells demonstrated excellent *in vitro* safety and efficacy. The viability results from the PLGA-ONBs-treated cells under hypoxia exhibited hypoxia recovery potential. Furthermore, the treatment of PLGA-ONBs did not induce a significant increase in ROS and SOD generation in cells. Additionally, the downregulation of hypoxic genes (HIF-1α, PAI-A, and VEGF-A) with PLGA-ONBs treatment (under hypoxia) exhibited hypoxia reversal potential at the cellular level. The safety study in the rabbit model further confirmed the potential applicability of PLGA-ONBs for intravitreal administration to mitigate retinal hypoxia. We propose the PLGA-ONBs as a promising candidate for retinal hypoxia reversal in ischemic retinal conditions, as well as an adjuvant in other diseases to mitigate hypoxia of the tumor microenvironment.

Author contributions

W. R. was responsible for the overall experimental design and formulation. W. R. and A. B. were responsible for data curation, formal analysis, preparation of the original draft, and editing of the revised manuscript. A. B., D. U., and X. H. performed the *in vitro* experiments. W. R. and J. I. were responsible for overall conceptualization. M. T. provided supervision and guidance. J. I. provided supervision, guidance on experimental planning, and funding. All authors contributed to the writing of the manuscript and have read and approved the manuscript.

Conflicts of interest

The authors declare no conflict of interest.

Ethical statement

All animal procedures were performed in accordance with the Guidelines for Care and Use of Laboratory Animals approved by the Animal Ethics Committee of the University of Illinois, Chicago, and strictly conformed to the Association for Research in Vision and Ophthalmology (ARVO) statement for the Use of Animals in Ophthalmic and Vision Research. All studies were conducted under the protocol number 24-096-Modification 01 approved by the Office of Animal Care and Institutional Biosafety (OACIB), University of Illinois, Chicago.

Data availability

The data supporting this article have been included as part of the SI. The SI containg comparison between fluorescent intensity of fluorescent PLGA-ONBs before and after dialysis, schemes for oxygen loading and releases, and photo of the test setup for the oxygen concentration measurement.

Supplementary information is available. See DOI: **https://doi.org/10.1039/d5bm01154j**.

Acknowledgements

This research was supported by the NSF-SBIR Award# 2236857. Partial seed funding from the Health Maker Lab (HML) of the Carle-Illinois College of Medicine is acknowledged.

References

1 N. N. Osborne, R. J. Casson, J. P. M. Wood, G. Chidlow, M. Graham and J. Melena, *Prog. Retinal Eye Res.*, 2004, **23**, 91–147.
2 A. S. Al-Kharashi, *Saudi J. Ophthalmol.*, 2018, **32**, 318–323.
3 S. S. Hayreh, *Prog. Retinal Eye Res.*, 2011, **30**, 359–394.
4 L. Zhang, F. Buonfiglio, A. Fieß, N. Pfeiffer and A. Gericke, *Antioxidants*, 2024, **13**, 148.
5 F. Menaa, B. A. Khan, B. Uzair and A. Menaa, *J. Multidiscip. Healthc.*, 2017, **10**, 335–346.
6 R. Wang, J. Xu, J. Xie, Z. Kang, X. Sun, N. Chen, L. Liu and J. Xu, *J. Neurotrauma*, 2010, **27**, 763–770.
7 Z. Micun, W. Dobrzyńska, M. Sieśkiewicz, I. Zawadzka, D. A. Dmuchowska, M. Wojewodzka-Zelezniakowicz and J. Konopińska, *J. Clin. Med.*, 2023, **13**, 29.
8 H. Di Vincenzo, A. Kauert, D. Martiano, J. Chiabo, D. Di Vincenzo, I. Sozonoff, S. Baillif and A. Martel, *Undersea Hyperbaric Med.*, 2022, **49**, 495–505.
9 O. Sayin and H. Altinkaynak, *Undersea Hyperbaric Med.*, 2022, **49**, 485–494.
10 M. Heyboer III, D. Sharma, W. Santiago and N. McCulloch, *Adv. Wound Care*, 2017, **6**, 210–224.
11 F. K. Butler Jr and C. Hagan, *Physiology and Medicine of Hyperbaric Oxygen Therapy*, 2008, vol. 71, pp. 565–572.
12 D. V. B. Batchelor, F. J. Armistead, N. Ingram, S. A. Peyman, J. R. Mclaughlan, P. L. Coletta and S. D. Evans, *Curr. Opin. Colloid Interface Sci.*, 2021, **54**, 101456.
13 S. M. Viafara Garcia, M. S. Khan, Z. S. Haidar and J. P. Acevedo Cox, *Nanomaterials*, 2023, **13**, 3060.
14 Y. Wang and T. Wang, *Coatings*, 2023, **13**, 1510.
15 K. Ohgaki, N. Q. Khanh, Y. Joden, A. Tsuji and T. Nakagawa, *Chem. Eng. Sci.*, 2010, **65**, 1296–1300.
16 F. Y. Ushikubo, T. Furukawa, R. Nakagawa, M. Enari, Y. Makino, Y. Kawagoe, T. Shiina and S. Oshita, *Colloids Surf., A*, 2010, **361**, 31–37.
17 W. Kanematsu, T. Tuziuti and K. Yasui, *Chem. Eng. Sci.*, 2020, **219**, 115594.
18 J. H. Weijs and D. Lohse, *Phys. Rev. Lett.*, 2013, **110**, 54501.
19 M. Alheshibri, J. Qian, M. Jehannin and V. S. J. Craig, *Langmuir*, 2016, **32**, 11086–11100.
20 G. Banche, V. Allizond, N. Mandras, N. Finesso, A. Luganini, T. Genova, M. Argenziano, C. Magnetto, G. R. Gulino, J. Roana, V. Tullio, G. Giribaldi, R. Cavalli, R. Spagnolo, A. Troia, A. M. Cuffini and M. Prato, *Toxicol. Rep.*, 2022, **9**, 154–162.
21 W. Wang, Y. Cheng, P. Yu, H. Wang, Y. Zhang, H. Xu, Q. Ye, A. Yuan, Y. Hu and J. Wu, *Nat. Commun.*, 2019, **10**, 1580.
22 G. Song, C. Ji, C. Liang, X. Song, X. Yi, Z. Dong, K. Yang and Z. Liu, *Biomaterials*, 2017, **112**, 257–263.
23 J. Jägers, A. Wrobeln and K. B. Ferenz, *Pflugers Arch.*, 2020, **473**, 139–150.
24 A. De, J.-P. Jee and Y.-J. Park, *Eur. J. Pharm. Biopharm.*, 2024, **199**, 114292.
25 P. Cabrales and J. M. Friedman, *Antioxid. Redox Signaling*, 2013, **18**, 2284–2297.
26 L. Song, G. Wang, X. Hou, S. Kala, Z. Qiu, K. F. Wong, F. Cao and L. Sun, *Acta Biomater.*, 2020, **108**, 313–325.
27 J. Owen, K. Logan, H. Nesbitt, S. Able, A. Vasilyeva, E. Bluemke, V. Kersemans, S. Smart, K. A. Vallis, A. P. McHale, J. F. Callan and E. Stride, *Nano Sel.*, 2021, **3**, 394–401.
28 L. Ye, L. Yang, X. Tan, P. Yang, Y. Liu, J. Peng, L. Zhao and Y. Zhou, *ACS Appl. Nano Mater.*, 2023, **6**, 11715–11724.
29 M. S. Khan, J.-S. Kim, J. Hwang, Y. Choi, K. Lee, Y. Kwon, J. Jang, S. Yoon, C.-S. Yang and J. Choi, *Theranostics*, 2020, **10**, 3892–3904.
30 R. Song, D. Hu, H. Y. Chung, Z. Sheng and S. Yao, *ACS Appl. Mater. Interfaces*, 2018, **10**, 36805–36813.
31 M. S. Khan, J. Hwang, Y. Seo, K. Shin, K. Lee, C. Park, Y. Choi, J. W. Hong and J. Choi, *Artif. Cells, Nanomed., Biotechnol.*, 2018, **46**, 318–327.
32 J. Tian, S. Wan, Z. Yang, M. Wang, W. Zhou, G. Wo, S. Fu, S. Zheng, G. Zhou, X. Hu, Y. Guo and J. Guo, *Adv. Healthcare Mater.*, 2024, **13**, 2400030.
33 J. Tian, S. Wan, J. Tian, L. Liu, J. Xia, Y. Hu, Z. Yang, H. Zhao, H. Wang, Y. Guo and J. Guo, *Small*, 2023, **19**, 2206091.
34 V. Messerschmidt, W. Ren, M. Tsipursky and J. Irudayaraj, *Transl. Vis. Sci. Technol.*, 2023, **12**, 16.
35 M. Fayyaz, M. Jabeen, M. S. Tsipursky and J. Irudayaraj, *ACS Appl. Nano Mater.*, 2021, **4**, 6583–6593.
36 R. Cavalli, A. Bisazza, P. Giustetto, A. Civra, D. Lembo, G. Trotta, C. Guiot and M. Trotta, *Int. J. Pharm.*, 2009, **381**, 160–165.
37 W. Ren, V. Messerschmidt, M. Tsipursky and J. Irudayaraj, *ACS Appl. Nano Mater.*, 2023, **6**, 13116–13126.
38 W. Ren, M. Sands, X. Han, M. Tsipursky and J. Irudayaraj, *ACS Omega*, 2024, **9**, 24095–24104.
39 Y. Su, B. Zhang, R. Sun, W. Liu, Q. Zhu, X. Zhang, R. Wang and C. Chen, *Drug Delivery*, 2021, **28**, 1397–1418.
40 B. Lu, X. Lv and Y. Le, *Polymers*, 2019, **11**, 304.
41 K. Park, S. Skidmore, J. Hadar, J. Garner, H. Park, A. Otte, B. K. Soh, G. Yoon, D. Yu, Y. Yun, B. K. Lee, X. Jiang and Y. Wang, *J. Controlled Release*, 2019, **304**, 125–134.
42 V. M. Gaspar, A. F. Moreira, E. C. Costa, J. A. Queiroz, F. Sousa, C. Pichon and I. J. Correia, *Colloids Surf., B*, 2015, **134**, 287–294.
43 C. Ke, T. Su, H. Chen, H. Liu, W. Chiang, P. Chu, Y. Xia and H. Sung, *Angew. Chem., Int. Ed.*, 2011, **50**, 8086–8089.
44 A. Raichur, Y. Nakajima, Y. Nagaoka, T. Maekawa and D. Sakthi Kumar, *Mater. Res. Express*, 2014, **1**, 045407.
45 Y. Cheng, J. Zhang, H. Nakano, N. Ueyama and H. Arakawa, *Mar. Pollut. Bull.*, 2023, **193**, 115167.
46 M. Suhail, C.-M. Shih, J.-Y. Liu, W.-C. Hsieh, Y.-W. Lin, I.-L. Lin and P.-C. Wu, *J. Drug Delivery Sci. Technol.*, 2022, **75**, 103715.
47 M. I. Koukourakis, A. Giatromanolaki, E. Sivridis, C. Simopoulos, H. Turley, K. Talks, K. C. Gatter and A. L. Harris, *Int. J. Radiat. Oncol., Biol., Phys.*, 2002, **53**, 1192–1202.

48 M. M. Hickey and M. C. Simon, *Current Topics in Developmental Biology*, Elsevier, 2006, pp. 217–257.
49 H. Liao, M. C. Hyman, D. A. Lawrence and D. J. Pinsky, *FASEB J.*, 2006, **21**, 935–949.
50 Y. Wu, Q. Zhang, D. K. Ann, A. Akhondzadeh, H. S. Duong, D. V. Messadi and A. D. Le, *Am. J. Physiol.: Cell Physiol.*, 2004, **286**, C905–C912.
51 H. Thangarajah, D. Yao, E. I. Chang, Y. Shi, L. Jazayeri, I. N. Vial, R. D. Galiano, X.-L. Du, R. Grogan, M. G. Galvez, M. Januszyk, M. Brownlee and G. C. Gurtner, *Proc. Natl. Acad. Sci. U. S. A.*, 2009, **106**, 13505–13510.
52 X. Han, L. Ju, M. Sands, Y. Zhao and J. Irudayaraj, *ACS Pharmacol. Transl. Sci.*, 2025, **8**, 602–612.